J. Fluid Mech. (2001), *vol.* 428, *pp.* 305–331. Printed in the United Kingdom

Fluid-loaded elastic plate with mean flow: point forcing and three-dimensional effects

By M. R. GREEN AND D. G. CRIGHTON†

Department of Applied Mathematics and Theoretical Physics, University of Cambridge, Silver Street, Cambridge, CB3 9EW, UK

(Received 1 July 1998 and in revised form 4 August 2000)

The unsteady behaviour of an infinitely long fluid-loaded elastic plate subject to a single-frequency line forcing in the presence of a uniform mean flow is known to exhibit a number of interesting phenomena. These include the onset of absolute instability for non-dimensional flow speeds U in excess of some critical speed U_c, and various interesting propagation effects when $U < U_c$. In the latter respect Crighton & Oswell (1991) have shown that over a particular frequency range there exists an anomalous neutral mode with group velocity directed towards the driver, in violation of the usual Lighthill outgoing radiation condition. Similar results have been found by Peake (1997) when transverse curvature effects are included. In this paper we seek to extend these results and consider the substantially harder problem of a fluid-loaded elastic plate with uniform mean flow which is subject to a point forcing, thereby resulting in a two-dimensional structural problem. A systematic method for determining the absolute instability threshold is developed, and it is shown that the flow is absolutely unstable for flow speeds $U > U_c$, where U_c is the one-dimensional value found by Crighton & Oswell. At flow speeds $U < U_c$ the flow is marginally stable and convective growth is found to occur downstream of the driver, over a particular frequency range depending on the transverse Fourier wavenumber k_y, within a wedge-shaped region. Outside this wedge-shaped region there is only neutral mode behaviour. Asymptotic forms are found for the dominant large-distance causal flexion response downstream of the driver inside and outside the wedge region, and the appropriate critical angle for the wedge region is identified. Within the convective instability wedge the flexion and critical angle take two different forms depending on whether the frequency ω is greater or less than $U^2/\sqrt{5}$. In addition to this interesting behaviour, the flow also exhibits the usual anomalous neutral mode behaviour and, as with Peake's problem, we also find an extra stability (hoop) resulting in neutral mode behaviour over a small frequency range. Asymptotic forms are also found for the threshold frequencies which divide up the various regions of stability of the system (neutral, neutral anomalous, convectively unstable), as a function of k_y, and are compared with the results of both Crighton & Oswell and Peake.

1. Introduction

The interaction between elastic structures and the surrounding fluid is very important when considering the design of large-scale engineering structures. This is especially important for marine applications where the fluid loading is significant. One main area of concern is the existence of damaging instabilities within the fluid–solid

† Sadly, Professor Crighton died during the publication process of this paper in April 2000.

system. These instabilities can arise due to various inhomogeneities (i.e. attachment points or rivets) in the solid body and can be transmitted into the fluid–solid system. This is particularly a problem where there is mean flow present and the instabilities can be severely damaging to the solid body.

There has been a lot of work done on the development and evolution of such instabilities within a number of analytically and numerically tractable scenarios. The early work of Benjamin (1960, 1963) and Landahl (1962) addressed the problem of an infinite compliant surface in the presence of an unsteady incompressible flow. The presence of negative energy waves was detected. Such waves decrease the total energy in the system and are destabilized by both plate dissipation and viscous effects (Cairns 1979). Recent work has revealed even more unusual behaviour within even the most (deceptively) simple model. Brazier-Smith & Scott (1984) considered an infinite elastic plate with mean flow and a single-frequency line forcing. The results obtained were numerical in nature. Crighton & Oswell (1991) analysed the same problem in great detail, and were able to derive an analytic solution of the problem. Both sets of authors used the spatial instability theory developed by Briggs (1964) and Bers (1983) for problems in plasma physics, and were able to show that the system is absolutely unstable for flow speeds in excess of a critical value U_c. For flow speeds less than U_c, various unusual propagation effects were shown to exist. In particular, Crighton & Oswell (1991) identify (in a parameter range in which all waves in the coupled system are neutrally stable) an anomalous neutral mode which, over a narrow frequency range, is found downstream of the driver but with negative group velocity (i.e. towards the driver), in violation of the usual outgoing wave condition at infinity. This is a reflection of the fact that the driver is not the only source of energy and that it may absorb energy from the reservoir provided by the mean flow, resulting in a negative rate of working for the driver over some frequency range.

The way in which such an apparently simple problem can exhibit such unusual behaviour has excited quite considerable interest. For instance, Abrahams & Wickham (1994) have used a similar analytical approach to the same infinite-plate problem, but with the inclusion of additional features such as dissipation in the plate, modified plate equations with improved high-frequency behaviour, and fluid compressibility. A recent paper by Peake (1997) extends the ideas of Crighton & Oswell (1991) to include the effect of transverse plate curvature. Initially the problem of uniform axial mean flow within a cylindrical shell was considered, but for large radius this approaches the problem of a flat plate with a modified plate equation incorporating an extra stiffness term. The problem was shown to exhibit all the interesting phenomena that arise for the flat plate problem, but the effect of stiffness is to increase the absolute instability threshold U_c to values well beyond speed ranges typically encountered in underwater applications. In addition, for some ranges of stiffness constant the anomalous neutral mode of Crighton & Oswell (1991) disappears altogether. A similar effect is also found where the plate has a continuous spring foundation or is of finite dimension.

The current paper is concerned with the response to localized point forcing of a fluid-loaded elastic plate when there is uniform flow over the plate. We adopt a similar approach to that used by Crighton & Oswell (1991) for the case of a fluid-loaded elastic plate subjected to line forcing, and comparisons are made with the work of both Peake (1997) and Crighton & Oswell (1991). Indeed, as with Peake's problem we find an extra stiffness-type term within a range of transverse wavenumbers, as well as all of the unusual behaviour associated with the one-dimensional flat plate problem. In this paper we do not seek to address the more 'realistic' case of boundary layer effects or finiteness. Although such effects are obviously important in real-world

applications, they introduce a level of complexity which would reduce the analytic tractability of the problem in question (which is already reasonably complex – see Lucey & Carpenter 1992). Indeed, even attempting to model a simple boundary layer in the form of a shear flow within the two-dimensional problem appears to be analytically complicated. Instead we choose to concentrate on the simplest problem incorporating three-dimensional effects, namely the effect of point forcing as opposed to line forcing.

The point forcing problem is somewhat harder in nature than the line forcing problem as we now have to consider a two-dimensional structural problem and a fully three-dimensional flow. The flow is taken to be along the positive x-direction and the transverse displacement (flexion) of the elastic plate is given by $z = \eta(x, y, t)$. When the variables are expressed in a suitably non-dimensional form (see Brazier-Smith & Scott 1984) we find that $\eta(x, y, t)$ satisfies

$$\left(\frac{\partial^2}{\partial t^2} + \left(\frac{\partial^2}{\partial x^2} + \frac{\partial^2}{\partial y^2}\right)^2\right)\eta(x, y, t) = F(t)\delta(x)\delta(y) - p(x, y, 0, t), \tag{1.1}$$

on $z = 0$. Only perturbations small enough to be described by linear theory are considered; x, y, z and t are space and time variables, p is the fluid pressure and F is the time-dependent strength of a point forcing function. The flow is assumed irrotational and incompressible and, as such, is specified by a potential $\phi(x, y, z, t)$ which satisfies Laplace's equation

$$\nabla^2\phi = 0, \tag{1.2}$$

throughout the fluid region. The pressure and potential are related by the linearized unsteady Bernoulli equation in the form

$$p = -\left(\frac{\partial\phi}{\partial t} + U\frac{\partial\phi}{\partial x}\right), \tag{1.3}$$

where U is the non-dimensional flow speed. There is also a kinematic condition, relating the potential and the flexion, in the form

$$\frac{\partial\phi}{\partial z}(x, y, 0, t) = \frac{\partial\eta}{\partial t} + U\frac{\partial\eta}{\partial x}. \tag{1.4}$$

For any function $g(x, y, t)$ we define its Fourier transform $\bar{g}(k_x, k_y, \omega)$ by

$$\bar{g}(k_x, k_y, \omega) = \int_{-\infty}^{\infty}\int_{-\infty}^{\infty}\int_{-\infty}^{\infty} g(x, y, t)\mathrm{e}^{\mathrm{i}(\omega t - k_x x - k_y y)}\mathrm{d}t\,\mathrm{d}x\,\mathrm{d}y. \tag{1.5}$$

Taking Fourier transforms in space and time (and assuming $F(t) = 0$ for $t < 0$), equations (1.1) to (1.4) may then be combined to give the causal solution of the problem in the form

$$\eta(x, y, t) = \frac{1}{8\pi^3}\int_{\Gamma_\omega} \Psi(x, y, \omega)\bar{F}(\omega)\mathrm{e}^{-\mathrm{i}\omega t}\mathrm{d}\omega, \tag{1.6}$$

where $\bar{F}(\omega)$ is the transform of $F(t)$, and

$$\Psi(x, y, \omega) = \int_{-\infty}^{\infty}\int_{-\infty}^{\infty} |k|\frac{\mathrm{e}^{\mathrm{i}(k_x x + k_y y)}}{D(k_x, k_y, \omega)}\mathrm{d}k_x\mathrm{d}k_y. \tag{1.7}$$

Here $k^2 = k_x^2 + k_y^2$, $|k| = \sqrt{k_x^2 + k_y^2}$, and

$$D(k_x, k_y, \omega) = |k|(k^4 - \omega^2) - (\omega - Uk_x)^2. \tag{1.8}$$

The spatial inversion (or k_x and k_y) contours are chosen to be the real k_x-axis and k_y-axis. In order to enforce causality, the temporal inversion (or ω) contour Γ_ω is chosen to be a straight line running parallel to the real ω-axis and lying above all the singularities in the ω-plane.

The integral (1.7) could be evaluated numerically for arbitrary (x, y, t) but this is cumbersome and very difficult, and reveals nothing of the physics. Instead we adopt the procedure used by Crighton & Oswell (1991) and concentrate on the large-time limit solution, which may be obtained analytically.

2. The large-time limit

The large-time asymptotics can be obtained by adapting the method of Briggs (1964) and Bers (1983) as explained in Brazier Smith & Scott (1984). Here it is the dispersion relation $D(k_x, k_y, \omega) = 0$ of the unforced problem that determines the solution to the forced problem. The idea is to slowly lower the ω contour down to the real ω-axis to obtain a causal solution in the form of a standard Fourier integral over real ω, whose integrand may then be regarded as the causal single-frequency response to single-frequency forcing initiated in the distant past. It is the behaviour of the poles of the integrand (i.e. the zeros of $D(k_x, k_y, \omega)$) that will now determine the nature of the response of the system to point forcing. However, unlike the line forcing problem (as examined by Crighton & Oswell 1991) we actually have two spatial integrations to perform and the Briggs–Bers method must be modified. The idea will be to first consider k_y as given and look at the k_x-integration. The presence of the k_y-variable introduces an extra degree of freedom, when deforming the k_x-contour. In fact, for any given streamwise group velocity $U_g = \partial\omega/\partial k_x$, the maximum growth rate with respect to spanwise group velocity $V_g = \partial\omega/\partial k_y$ occurs with $\mathrm{Im}(k_y) = 0$. This can also be seen in related experiments on infinite thin plates (Lucey & Carpenter 1992). We could therefore consider k_y as real at this stage. Once the k_x-integral has been performed, the k_y-integral can then be calculated using the method of steepest descent.

Thus we first consider the zeros of $D(k_x, k_y, \omega)$ in the form $k_x \equiv k_x(k_y, \omega)$, where k_y and ω are given. As the temporal contour Γ_ω is deformed down toward the real ω-axis, the poles of the integrand in the k_x-plane (zeros of $D(k_x, k_y, \omega) = 0$) are caused to move around. The k_x-contour must then be deformed off the real axis to prevent any poles from crossing it, if a causal solution (and the necessary corresponding analytic continuation of the Ψ function) is to be maintained. There are essentially four possible scenarios that need to be considered.

(*a*) The contour Γ_ω may be deformed down onto the real ω-axis without any poles crossing the real k_x-axis. Any poles that come to rest on the real k_x-axis will need to have the k_x-contour indented above or below them, depending on which half-plane they originated in. Then, such poles originating in the upper half-plane represent neutral wave modes found downstream whilst those originating in the lower-half plane represent neutral modes found upstream.

(*b*) A pole from the upper half-k_x-plane crosses over into the lower half-k_x-plane as Γ_ω is lowered. This requires the k_x-contour to be deformed downward, so that a convectively unstable wave is then found downstream of the forcing (in $x > 0$).

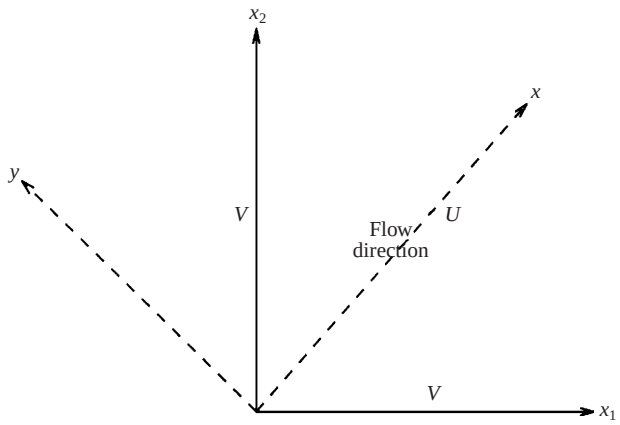

FIGURE 1. Rotation from (x, y)-axes to (x_1, x_2)-axes.

(c) A pole from the upper half-k_x-plane crosses the real k_x-axis as Γ_ω is lowered, but then turns round and moves back up onto the real axis as Γ_ω approaches the real ω-axis. Such a neutral mode will again be found downstream (since it originated in the upper half-plane), but it now has a negative group velocity (directed towards the line forcing). Such modes are usually referred to as anomalous modes of propagation and have been discussed in great depth by Crighton & Oswell (1991).

(d) Finally, if two or more poles coalesce or pinch the k_x-contour off the real k_x-axis, as Γ_ω is being lowered toward the real ω-axis, the flow is said to be absolutely unstable. It can be shown that such a situation gives rise to a growth in time proportional to $\exp(-\mathrm{i}\omega_p t)$ at any fixed location, where ω_p is the complex frequency at which the pinch occurs in the k_x-plane (as Γ_ω is lowered) with $\mathrm{Im}(\omega_p) > 0$.

All four of these possible types of behaviour (as found by Crighton & Oswell (1991) for line-forcing, $k_y = 0$) are also found to exist in our point forcing problem. We concentrate first on the possibility of absolute instability arising.

3. The existence of absolute instability

We will now try to deduce the existence of an instability threshold in a similar manner to that adopted by Crighton & Oswell (1991) for the one-dimensional structural problem of a plate with mean flow. It will be shown that for a two-dimensional structural problem we can calculate the threshold for absolute instability in terms of the limiting case of a saddle point. From §1, the dispersion function arising from flow in the x-direction is given by

$$D(k_x, k_y, \omega) = |k|(k^4 - \omega^2) - (\omega - Uk_x)^2. \tag{3.1}$$

However, to analyse the absolute instability it is more useful to consider the flow in a new set of axes (x_1, x_2) at an angle of $\pi/4$ to the original axes, as shown in figure 1. Then in terms of the new axes we have a flow speed $V = U/\sqrt{2}$ in both the x_1- and x_2-directions, and the dispersion function is now

$$D_1(k_1, k_2, \omega) = |k|(k^4 - \omega^2) - (\omega - V(k_1 + k_2))^2, \tag{3.2}$$

with $D_1(k_1, k_2, \omega) = D(k_x, k_y, \omega)$ and (k_1, k_2) transform variables conjugate to (x_1, x_2). By comparison with the one-dimensional structural problem, an absolute instability

can only arise at a saddle point (also corresponding to a double root of the dispersion relation). In two dimensions we thus require

$$\frac{\partial D_1}{\partial k_1} = 0, \qquad \frac{\partial D_1}{\partial k_2} = 0, \tag{3.3}$$

or equivalently $\partial\omega/\partial k_1 = 0$ and $\partial\omega/\partial k_2 = 0$, for a non-zero flow speed V and frequency ω. Applying these conditions to (3.2) leads to

$$(5k^4 - \omega^2)\frac{k_1}{|k|} + 2V(\omega - V(k_1 + k_2)) = 0, \tag{3.4}$$

$$(5k^4 - \omega^2)\frac{k_2}{|k|} + 2V(\omega - V(k_1 + k_2)) = 0, \tag{3.5}$$

together with (3.2) itself. Eliminating the first term between (3.4) and (3.5) gives

$$2V(k_1 - k_2)(\omega - V(k_1 + k_2)) = 0, \tag{3.6}$$

which for non-zero flow speed V requires

$$\omega = V(k_1 + k_2) \quad \text{or} \quad k_1 = k_2. \tag{3.7}$$

Assuming $k_1 \neq k_2$ gives $\omega = V(k_1 + k_2)$. However, substituting this value of ω back into the dispersion relation and (3.4) and (3.5) reveals that $\omega = 0$ is the only solution, and so does not give rise to an absolute instability. Therefore we must have $k_1 = k_2$, as indeed might be expected from symmetry. Substituting $k_1 = k_2$ within (3.2) and one of (3.4) or (3.5), together with $k = \sqrt{2}k_1 = \sqrt{2}k_2$ and $U = \sqrt{2}V$, leads to

$$(k^4 - \omega^2)|k| - (\omega - Uk)^2 = 0, \tag{3.8}$$

$$(5k^4 - \omega^2) + 2U(\omega - Uk) = 0, \tag{3.9}$$

where $|k| = k\,\mathrm{sgn}(\mathrm{Re}(k))$ now. These two equations are instantly recognizable as those associated with the elastic plate with line forcing (as examined by Crighton & Oswell 1991) with one-dimensional dispersion function $D_2(k, \omega) = (k^4 - \omega^2)|k| - (\omega - Uk)^2$, and the double root condition $\partial D_2/\partial k = 0$.

In fact, equations (3.8) and (3.9) contain enough information to deduce the critical velocity U_c numerically. Indeed, it is possible to eliminate ω from them, resulting in a seventh-order polynomial in k and U. We consider $\mathrm{Re}(k) > 0$ and $\mathrm{Re}(k) < 0$ separately and solve for k numerically as U is slowly increased, discarding solutions that lie in the 'wrong' half-plane. The allowable solutions will give rise to the values of ω associated with the turning points ($\partial\omega/\partial k = 0$), which may then be plotted as a function of U, with the coalescence of a maximum and minimum again representing the merging of three roots and so identifying the critical velocity U_c, as first discussed by Crighton & Oswell (1991). Then, since the equations (3.8) and (3.9) are identical to those found by Crighton & Oswell, the critical value U_c must also be the same as previously found. We could also identify the critical velocity U_c directly by differentiating equation (3.9) with respect to k (so giving the triple root condition $\partial^2 D_2/\partial k^2 = 0$ as given by Crighton & Oswell for the one-dimensional structural problem).

For a one-dimensional problem with dispersion function D_2 say, defined above, it is clear that the condition $\partial^2 D_2/\partial k^2 = 0$ corresponds to a triple root. Applying such a condition to (3.8) would give the correct result, but for our problem $k^2 = k_1^2 + k_2^2$, and there is no easy interpretation of the meaning of this condition. Instead we recall that for the one-dimensional problem, the triple root condition also means

that the dispersion function has an inflection point. The analogous statement for two dimensions involves the limiting case of a saddle, as given by the vanishing of the discriminant

$$\Delta \equiv \left(\frac{\partial^2 D_1}{\partial k_1 \partial k_2}\right)^2 - \frac{\partial^2 D_1}{\partial k_1^2}\frac{\partial^2 D_1}{\partial k_2^2} = 0. \tag{3.10}$$

Applying this to the dispersion relation (3.2), substituting $k_1 = k_2$ at the saddle, and rewriting in terms of k, gives

$$(5k^4 - \omega^2)(V^2 - 5k^3) = 0 \quad \text{for } \mathrm{Re}(k) > 0. \tag{3.11}$$

The solution $5k^4 - \omega^2 = 0$, when combined with (3.8) and (3.9), reveals $\omega = 0$ as the only possible solution again, and does not give an absolute instability. Therefore we must have

$$(V^2 - 5k^3) = 0, \quad \text{or} \quad k^3 = \frac{U^2}{10}. \tag{3.12}$$

This is exactly the value of k predicted by Crighton & Oswell (1991) for the one-dimensional structural problem, and since (3.8) and (3.9) are also identical to those for that problem we must have the same value for the instability threshold $U = U_c$, namely

$$U_c = \frac{5^{5/4}2^{1/2}}{3^{3/4}}\left(2 - \frac{15^{1/2}}{2}\right)^{3/2} \approx 0.074. \tag{3.13}$$

Thus we have found a more satisfactory way of deducing the result (which was expected on numerical grounds from equations (3.8) and (3.9) alone) than by simply applying a condition $\partial^2 D_2/\partial k^2 = 0$, which has no obvious interpretation for a two-dimensional dispersion relation.

Now that the threshold for absolute instability has been deduced it is more convenient to work with a coordinate system where the flow is in the x-direction and with the dispersion function $D(k_x, k_y, \omega)$ as given by (1.8). In terms of these coordinates the direction $k_1 = k_2$ is along the flow direction (now the x-direction, as in figure 1). The above results then imply that the critical velocity U_c occurs for $k_y = 0$, and that all other k_y must have a higher critical velocity associated with them. In fact one can expand (1.8), treating k_y as a small parameter, and applying the Crighton & Oswell result for a triple root; one finds an equation that must be satisfied by the critical velocity U_y associated with a given small k_y,

$$k_y^2 = \tfrac{2}{15}U_y^{4/3}(U_y^{2/3} - U_c^{2/3}), \tag{3.14}$$

or, explicitly for U_y, in terms of k_y,

$$U_y = U_c\left(1 + \frac{45}{4U_c^2}k_y^2 + O(k_y^4)\right), \tag{3.15}$$

with U_c as in (3.13). It is clearly seen that for any small non-zero k_y the associated critical velocity U_y is larger than the threshold velocity U_c derived above. Since the inversion integration is over all k_y, we must pick the lowest value $U = U_c$ as the threshold, to avoid an absolute instability occurring. We now consider the possibility of the flow exhibiting convective instabilities, using a modified form of the Briggs–Bers analysis.

4. Convectively stable and unstable flow

In this section we suppose that $U < U_c$, so that the flow can be at worst convectively unstable, and the Briggs–Bers method can potentially exhibit the behaviour (*a*), (*b*) or (*c*) described in § 2. Since $U < U_c$ we can now safely lower the contour Γ_ω all the way down onto the real ω-axis, and we need only consider real frequencies in what follows. At this point we still consider the k_y-contour as running along the real k_y-axis and look at the trajectories of the zeros of $D(k_x, k_y, \omega)$ within the complex k_x-plane, for k_y and ω given. In fact, we may consider a definite forcing function with frequency ω_0 (which is still arbitrary), given by $F(t) = F_0 e^{-i\omega_0 t}$, for $t > 0$. Then, performing the temporal inversion in equation (1.6) gives the flexion $\eta(x, y, t)$ in the form

$$\eta(x, y, t) = \frac{F_0}{4\pi^2} \Psi(x, y, \omega_0) e^{-i\omega_0 t}, \tag{4.1}$$

with Ψ now given by

$$\Psi = \int_{-\infty}^{\infty} e^{ik_y y} \left(\int_c \frac{|k| e^{ik_x x}}{D(k_x, k_y, \omega_0)} dk_x \right) dk_y, \tag{4.2}$$

where the c contour has been deformed to allow for a causal solution in the usual Briggs–Bers manner. Expression (4.2), the residue from the pole at $\omega = \omega_0$, is the $O(1)$ dominant asymptotic contribution as $t \to \infty$; in addition to (4.2) there are residues from poles in $\mathrm{Im}(\omega) < 0$ and from branch points in $\mathrm{Im}(\omega) \leqslant 0$, all of which decay algebraically or faster as $t \to \infty$. Dropping the suffix from ω_0 now, the deformation of c will depend on the values of k_y and ω, which determine how the zeros of the dispersion function $D(k_x, k_y, \omega)$ move in the k_x-plane as the real frequency ω is attained. Note that if we take $\omega \to -\omega$ and $k_x \to -k_x$ the dispersion relation (1.8) remains unchanged. Therefore we restrict our analysis to positive frequencies ω only.

If we consider (1.8) and solve for ω as a function of k_x (with k_y treated as a real parameter at this stage), we find two possible branches,

$$\omega_\pm = \frac{U k_x \pm \sqrt{k^6 + |k|(k^4 - U^2 k^2 + U^2 k_y^2)}}{1 + |k|}. \tag{4.3}$$

The square-root term $|k|$ is defined to behave like

$$\begin{aligned} |k| &\sim k_x \quad \text{as} \quad k_x \to \infty \\ |k| &\sim -k_x \quad \text{as} \quad k_x \to -\infty, \end{aligned} \tag{4.4}$$

so that as $k_y \to 0$, $\omega_\pm$ give the Crighton & Oswell results for a line-forced plate. Quite often we will use k to denote $|k|$, and the two are often used interchangeably.

It is helpful to consider the branches of $\omega_\pm(k_x; k_y, U)$ for different values of k_y, as plotted in figure 2 with $U = 0.05$. The value $k_y = 0$ (part *a*) gives the one-dimensional results of Crighton & Oswell (1991) (for that $U = 0.05$). In their problem, it was demonstrated that at frequencies less than ω_{min} associated with the local minimum in $\mathrm{Re}(k_x) > 0$ (as shown in figure 3 for our problem) convective instability occurs. That is, for $\omega < \omega_{min}$ two of the roots $k_x = k_x(\omega, U)$ are complex. However, if we slowly increase k_y up to $k_y = 0.02$ (figure 2*b*) it becomes apparent that we now also get two real roots, with small k_x and ω. Indeed, increasing k_y still further up to (*c*) $k_y = 0.0245$ results in a larger region over which these neutral modes are obtained (and hence a smaller convective instability region). This new region of stability is often referred to as a stability hoop and has also been found in the problem of a fluid-loaded cylindrical shell with mean flow (Peake 1997). Finally in (*d*), with $k_y = 0.03$, the

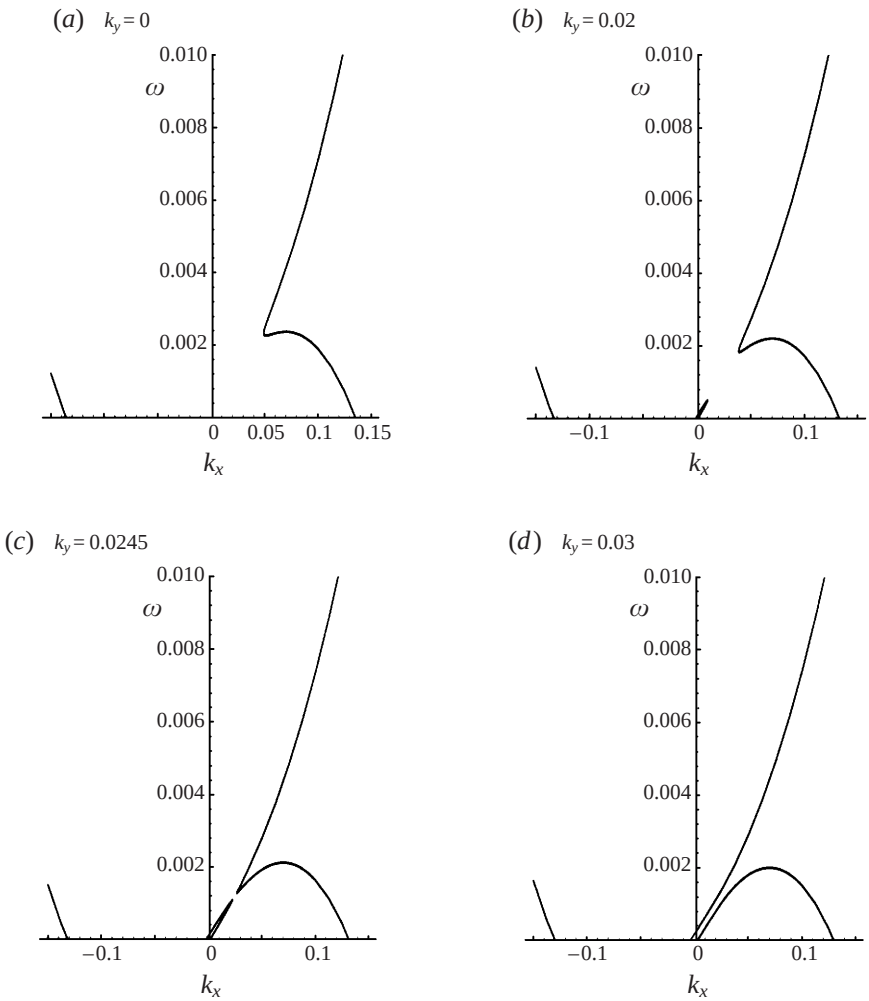

FIGURE 2. Real solutions k_x of the dispersion relation for a range of real ω and selected real values of k_y.

convective instability region has completely disappeared leaving four neutral modes. It is interesting that the convective instability region should only exist for small values of k_y. This suggests that some form of asymptotic analysis should be possible for small k_y.

4.1. *Branch point and turning point analysis*

Differentiating (4.3), the group velocity is

$$\frac{\partial \omega}{\partial k_x} = \frac{2UA^{1/2}(k + k_y^2) \pm k_x B}{2(1+k)^2 A^{1/2} k} \tag{4.5}$$

where

$$\left.\begin{aligned} A &= k^6 + k^5 - k k_x^2 U^2, \\ B &= 4k^6 + 9k^5 + 5k^4 - k^3 U^2 - 3k^2 U^2 + (1-k) U^2 k_y^2. \end{aligned}\right\} \tag{4.6}$$

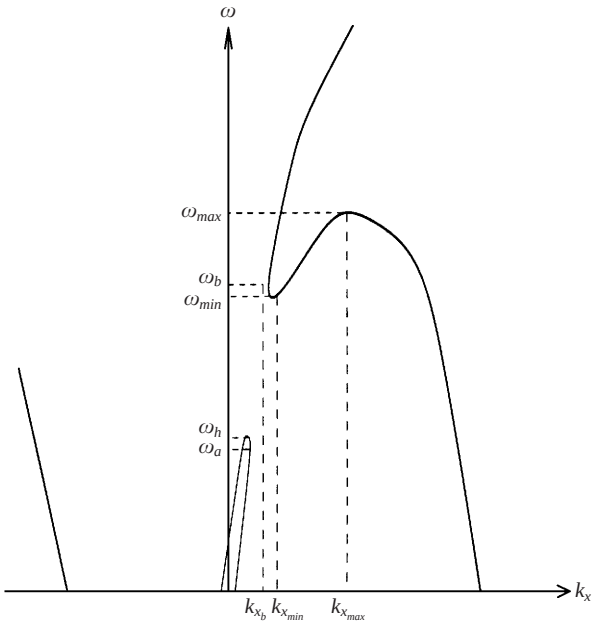

FIGURE 3. Schematic representation for $\omega = \omega(k_x)$, with $k_y < U/2$ and $U = 0.05$.

The branch point frequency is that at which $\partial\omega/\partial k_x$ becomes infinite. This occurs when A vanishes (for real values of k_x), that is where

$$k^6 + |k|k^4 - |k|U^2k_x^2 = 0. \tag{4.7}$$

The branch point for both Peake's (1997) and Crighton & Oswell's (1991) results was found to arise when $k = O(U)$. With this in mind we set $k_x = UK_x$ and $k_y = UK_y$ as the appropriate scaling, so that $k = UK$ now. Then, recalling that $U_c \ll 1$, so that $U \to 0$ is an appropriate asymptotic limit, we find from (4.7) that

$$K_x = \frac{1 \pm \sqrt{1 - 4K_y^2}}{2} \tag{4.8}$$

to leading order (with $\mathrm{Re}(K_x) > 0$) and so we obtain real solutions provided $K_y < 1/2$. In terms of the original variables, this condition is $k_y < U/2$. Note in figure 2 that the transition from a convective instability region to one having all modes neutral occurred between $k_y = 0.0245$ and $k_y = 0.03$, with $U = 0.05$. In fact a closer inspection reveals that the transition does indeed occur for the value of $k_y = U/2 = 0.025$ (to leading order). Denoting the branch points on the hoop and main region, respectively, by K_{x_a} and K_{x_b}, we then have

$$K_{x_a,x_b} = \frac{1 \mp \sqrt{1 - 4K_y^2}}{2}, \tag{4.9}$$

where the smaller root is associated with the stability hoop region (and vanishes when $k_y = 0$). The branch frequencies $\omega_{a,b}$ associated with these wavenumbers are then

$$\omega_{a,b} = \frac{U^2K_{x_a,x_b}}{1 + U\sqrt{K_{x_a,x_b}}}. \tag{4.10}$$

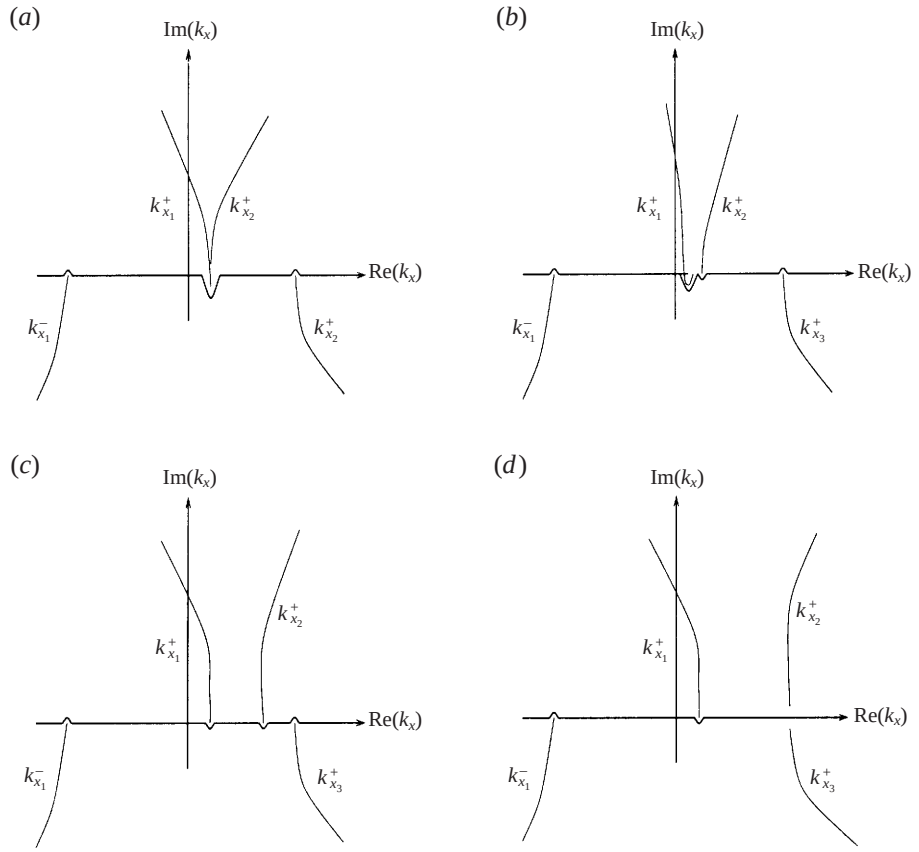

FIGURE 4. Root tracing for (*a*) $\omega_h < \omega < \omega_{min}$, (*b*) $\omega_{min} < \omega < \omega_b$, (*c*) $\omega_b < \omega < \omega_{max}$ and (*d*) $\omega_{max} < \omega$, with $U = 0.05$.

In the limit $k_y \to 0$ it is seen that $K_{x_b} \to 1$, so that we obtain the branch frequency of Crighton & Oswell, $\omega_b = U^2/(1+U)$.

The existence of a branch point coincides with the existence of both a local minimum, denoted by ω_{min}, and a local maximum, ω_{max} (although the local maximum can exist without the branch point, as in figure 2(*d*)). Thus we assume $k_y < U/2$, so that both ω_{min} and ω_{max} exist. Applying a full Briggs–Bers-type analysis (which is necessarily numerical in nature) the behaviour of the roots in the k_x-plane may be traced as Γ_ω is lowered to the real axis. At frequencies $\omega < \omega_{min}$ (figure 4(*a*)) it is found that there is the possibility of a convectively unstable mode existing downstream of the driver (with two neutral modes upstream and one evanescent mode downstream). Note, however, that unlike the Crighton & Oswell case, it is no longer the whole region $\omega < \omega_{min}$ that gives rise to convective instability. Indeed, for non-zero values of $k_y < U/2$ there is a local maximum associated with the hoop (ω_h say), so that the convectively unstable region exists only for $\omega_h < \omega < \omega_{min}$ now. At frequencies $\omega < \omega_h$ there are four neutral modes (with the two neutral modes arising from the stability hoop appearing downstream).

At frequencies $\omega_{min} < \omega < \omega_{max}$ there are four neutral modes – two upstream and two downstream. The behaviour of the various modes in this region depends further on the branch frequency ω_b. At frequencies $\omega_{min} < \omega < \omega_b$ there exists an anomalous

neutral mode also found by Crighton & Oswell (1991) and Peake (1997). This is shown in figure 4(*b*) where the root $k_{x_1}^+$, which originates in the upper half-k_x-plane, dips below the real k_x-axis but finishes on it, as Γ_ω is lowered to the real ω-axis. This mode is therefore found downstream but has the unusual characteristic of a negative group velocity, directed towards the driver. Such behaviour has already been well documented and examined in great detail by Crighton & Oswell, and thus we will not examine it any further in this paper – merely noting that it does exist (when the branch frequency exists) for the present two-dimensional structural problem as well. At frequencies $\omega_b < \omega < \omega_{max}$ (figure 4 (*c*)) we have four neutral modes with the usual propagation characteristics, and at frequencies $\omega > \omega_{max}$ there exist two neutral modes, one upstream and one downstream, and two evanescent modes, one upstream and one downstream.

Since both k_y and U are small, it is possible to derive asymptotic forms for the turning-point wavenumbers and frequencies (where k_y is considered as given and $k_y < U/2$). From (4.5) it follows that the condition for the existence of turning points is

$$U^2 = \frac{k_x^2 FH + 2G(k+k_y^2)^2}{k_x^2 H^2 + 4(k+k_y^2)^2 k k_x^2}\left(1 \pm \sqrt{1 - \frac{k_x^2 F^2 (k_x^2 H^2 + 4(k+k_y^2)^2 k k_x^2)}{(k_x^2 FH + 2G(k+k_y^2)^2)^2}}\right), \tag{4.11}$$

where

$$F = 4k^6 + 9k^5 + 5k^4, \quad G = k^6 + k^5, \quad H = k^3 + 3k^2 + (k-1)k_y^2. \tag{4.12}$$

Scaling $k_x = UK_x$ and $k_y = UK_y$ and expanding to leading order, we find the K_x given in (4.8). The larger root gives the value of k_x at the local minimum ω_{min} and the smaller root gives the value of k_x at the local maximum on the stability hoop branch and tends to zero as $k_y \to 0$. From (4.3) it follows that the frequency associated with the positive root is

$$\omega_{min} = \frac{U^2(1 + \sqrt{1 - 4K_y^2})}{2}, \tag{4.13}$$

to leading order in U. Note that this is the same as the branch-point frequency ω_b to leading order (equation (4.10)). It is obvious from figure 3 that $\omega_b > \omega_{min}$, implying that (4.13) overpredicts the value associated with ω_{min} to leading order and, as Crighton & Oswell observed, it is necessary to go to second order to obtain accurate results. It is demonstrated later how the correction to the frequency may be obtained in a more systematic manner (involving less algebra) by examining the convective instability modes themselves, and we do not pursue the matter as such further here.

To examine the larger turning point (associated with ω_{max}) a different scaling of k_x is required. We keep the same scaling for k_y – which is necessary for the existence of a convective region (and hence the existence of both turning points). It was demonstrated by Crighton & Oswell that the appropriate scaling for the line-forced plate was $k_x = O(U^{2/3})$ and since k_y is small by comparison we adopt a similar scaling. Thus scaling $k_x = U^{2/3}K_x$, with $k_y = UK_y$ still, and expanding equation (4.11) to second order in terms involving K_x (while still only retaining leading-order terms in K_y), it is found that

$$K_{x_{max}} \sim \left(\frac{4}{25}\right)^{1/3} + \frac{U^{2/3}}{3}\left(\frac{49}{10}\left(\frac{4}{25}\right)^{2/3} - \frac{K_y^2}{2(4/25)^{1/3}}\right). \tag{4.14}$$

Again, it follows from (4.3) that the associated value of the frequency is given by

$$\omega_{max} = U^{5/3}\left(\frac{4}{25}\right)^{1/3} + \frac{U^{2/3}}{3}\left(\frac{49}{10}\left(\frac{4}{25}\right)^{2/3} - 3\left(\frac{4}{25}\right)^{1/3} - \frac{K_y^2}{2(4/25)^{1/3}}\right). \tag{4.15}$$

Note that it was necessary to expand to second order to get any significant effect involving K_y. In the limit $K_y \to 0$, (4.14) and (4.15) tend to the results of Crighton & Oswell (1991) for a line-forced plate, and the term involving K_y can therefore be regarded as a small correction to their result.

4.2. *Modal analysis*

Since both k_y and U are small within the convectively unstable region (which will dominate any large-distance solution) it should be possible to derive asymptotic forms for the various modes. With this in mind we consider k_x and k_y now again both of order U (with $k_y < U/2$ so that the convective region exists), and scale the frequency appropriately so that it is possible to derive asymptotic forms for the convective roots. In order to balance the inertial and mean flow terms we must set $\omega \sim O(Uk)$. Thus we scale $\omega = U^2\Omega$ along with $(k_x, k_y, k) = U(K_x, K_y, K)$ in the dispersion function (1.8). Then we find two roots

$$K^+_{x_{1,2}} = \Omega \pm U^{1/2}(\Omega^2 + K_y^2)^{1/4}(\Omega^2 + K_y^2) + \Omega)^{1/2}(\Omega^2 + K_y^2 - \Omega)^{1/2} + O(U). \tag{4.16}$$

If we define $g(K_y, \Omega) = \Omega^2 + K_y^2 - \Omega$, the instability boundary may be identified by $g = 0$. For $g < 0$ the two roots in (4.16) become complex (and give rise to a convective instability), and for $g > 0$ there are two real roots (corresponding to two neutral waves). The two roots of $g = 0$ are

$$\Omega_\pm = \frac{1 \pm \sqrt{1 - 4K_y^2}}{2}, \tag{4.17}$$

with $g < 0$ for $\Omega_- < \Omega < \Omega_+$. It is immediately apparent that these are the same two roots derived in the previous section, corresponding to the local maximum on the stability hoop and the local minimum on the main flow region (denoted by ω_{min}) but now expressed in rescaled form (i.e. Ω_{min}). Thus, at frequencies within this range the flow may exhibit convective instabilities. In the previous section it was remarked that the value of ω_{min} (and hence Ω_{min}) was over-estimated by the above leading-order approximation. It is possible to find an appropriate form for the correction to the stability boundary $g = 0$ by finding the higher-order terms for the convective modes. Expanding the dispersion relation to higher order, it can be shown that the convective roots take the form

$$\begin{aligned} K^+_{x_{1,2}} = {} & \Omega \pm U^{1/2}(\Omega^2 + K_y^2)^{1/4}(\Omega^2 + K_y^2) + \Omega)^{1/2}(\Omega^2 + K_y^2 - \Omega)^{1/2} \\ & + U\frac{\Omega\left(5(\Omega^2 + K_y^2)^2 - \Omega^2\right)}{2(\Omega^2 + K_y^2)^{1/2}} \pm U^{3/2}\frac{\Omega^2(5(\Omega^2 + K_y^2)^2 - \Omega^2)^2}{8(\Omega^2 + K_y^2)^{5/4}((\Omega^2 + K_y^2)^2 - \Omega^2)^{1/2}} \\ & \pm U^{3/2}((\Omega^2 + K_y^2)^2 - \Omega^2)^{1/2}\left(5\Omega^2(\Omega^2 + K_y^2)^{3/4} + \frac{(5(\Omega^2 + K_y^2)^2 - \Omega^2)K_y^2}{4(\Omega^2 + K_y^2)^{5/4}}\right) \\ & + O(U^2). \end{aligned} \tag{4.18}$$

Here the fourth term may be interpreted as a shift in the neutral position defined to lowest order by the second term, with the function g now defined by

$$g = \Omega^2 + K_y^2 - \Omega + \frac{U}{4}\frac{\Omega^2(5(\Omega^2+K_y^2)^2-\Omega^2)^2}{(\Omega^2+K_y^2+\Omega)^{1/2}(\Omega^2+K_y^2)^{3/2}}. \tag{4.19}$$

The condition $g = 0$ (with K_y given) gives the corrected version for the upper (i.e. Ω_{min}) and lower (i.e. Ω_h) instability boundaries, respectively, in the form

$$\Omega_{min} \sim \Omega_+ - \frac{2U\Omega_+^{7/2}}{2\Omega_+ - 1}, \tag{4.20}$$

$$\Omega_h \sim \Omega_- + \frac{2U\Omega_-^{7/2}}{1 - 2\Omega_+}, \tag{4.21}$$

where $\Omega_\pm$ are defined in (4.17) above. The roots defined in (4.18) are complex in the region $\Omega_h < \Omega < \Omega_{min}$. Performing the usual Briggs–Bers lowering of the temporal contour it is found that both roots originate in the upper half-k_x-plane, and are therefore found downstream of the driver, and that it is the root with negative imaginary part (denoted by K_{x_1} in keeping with figure 4) that causes exponential growth downstream (giving rise to convective instability).

From the dispersion relation analysis of the previous section, when $k_y < U/2$ there are also two neutral modes found upstream of the driver. Keeping the same scaling for k_y (hence retaining the existence of the convective region) and ω, it is found that the appropriate scaling for k_x is now $k_x = U^{2/3}K_x$. Substituting in (1.8) and expanding we find the two larger roots in the form

$$\left.\begin{aligned} K_{x_1}^- &\sim -1 - U^{1/3}\frac{2\Omega}{3} + U^{2/3}\left(\frac{5\Omega^2}{9} + \frac{5K_y^2}{6}\right), \\ K_{x_3}^+ &\sim 1 - U^{1/3}\frac{2\Omega}{3} - U^{2/3}\left(\frac{5\Omega^2}{9} + \frac{5K_y^2}{6}\right). \end{aligned}\right\} \tag{4.22}$$

So far we have assumed k_y as given and derive a frequency range ($\Omega_h < \Omega < \Omega_{min}$) for the existence of a convective instability region . However, it transpires that to obtain an asymptotic form for the large-distance solution it is necessary to consider Ω as given and interpret the existence of the convective instability region in terms of a restriction on the values that k_y can take. This is easily obtained from the instability threshold $g = 0$, resulting in a convective instability provided $|K_y| < K_0$, where

$$K_0 = (\Omega - \Omega^2 - 2U\Omega^{7/2})^{1/2}. \tag{4.23}$$

In fact, within the analysis that follows, the leading-order approximation is sufficient, so that $K_0 = (\Omega - \Omega^2)^{1/2}$. Note that K_0 is real provided $0 < \Omega < 1$, with maximum value of $K_y = 1/2$ at $\Omega = 1/2$. The effect of increasing K_y has already been examined in figure 2. Consider $|K_y| \ll K_0$; then there exists a range of frequencies for Ω lying in $(0, 1)$ (the exact range depending on the value of K_y given) which give rise to a convectively unstable mode downstream. In addition there also exists a conjugate mode which is exponentially decaying downstream. As K_y is increased up to the value $|K_y| = K_0$ the exponentially decaying and growing modes merge and become neutral – either on the main stability branch (figure 2) when $\Omega > 1/2$, or on the hoop branch when $\Omega < 1/2$. The choice $\Omega = 1/2$ corresponds to the transition from convective to neutral wave modes occurring at $K_y = 1/2$, when the stability hoop region and the

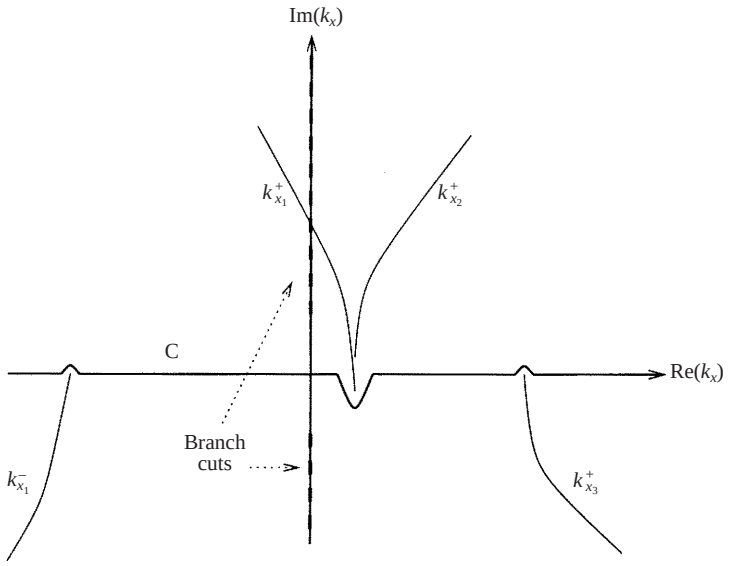

FIGURE 5. Integration path C for convectively unstable region.

main neutral region merge. That is, $\Omega = 1/2$ results in the largest region of convective instability that is possible in terms of range of K_y.

4.3. *Large-distance solution*

The asymptotic form of the convective instabilities is now known as a function of k_y, ω and U, as is the range of values of k_y for such convective instabilities to exist. It should therefore be possible to obtain an asymptotic form for the flexion associated with the convective instability region. The idea is to split the range of k_y-integration into three regions: $(-\infty, U/2)$, $(U/2, \infty)$ and $(-U/2, U/2)$. The first two regions can only contain neutral waves (at worst) and evanescent waves (which are ignored within the large-distance solution). The region $(-U/2, U/2)$, however, can give rise to convective growth. In the current analysis we concentrate on this convective instability region (which will dominate any large-distance solution anyway). For a given frequency (with $0 < \omega < U^2$) we perform the k_x-integration using the residue theorem (with dominant contribution from the convective instability wave) and then use a steepest descent method applied to the k_y-integral which remains.

Formally we have the solution in the large-time asymptotic limit as given by (4.1) and (4.2). In terms of the unscaled variables, the convective instability region only occurs for $-UK_0 < k_y < UK_0$. As such, the leading-order contribution for large distances to the Ψ function of (4.2) comes from this region. Introducing the scaled variables K_x, K_y, K and Ω as before (scaled on U and U^2 respectively) the dominant contribution to Ψ is given by

$$\Psi \sim \frac{1}{U}\int_{-K_0}^{K_0}\int_c \frac{K\mathrm{e}^{\mathrm{i}U(K_x x + K_y y)}}{-(K_x-\Omega)^2 + UK(K^4-\Omega^2)}\mathrm{d}K_x\mathrm{d}K_y. \tag{4.24}$$

Applying the Briggs–Bers analysis reveals that the contour c must be deformed as shown in figure 5 if one is to obtain an analytic continuation. Note that there are two branch cuts associated with $K = 0$, so that cuts are taken from $K_x = \pm\mathrm{i}|K_y|$ to infinity, as shown. Closing the contour in the upper half-plane then gives rise

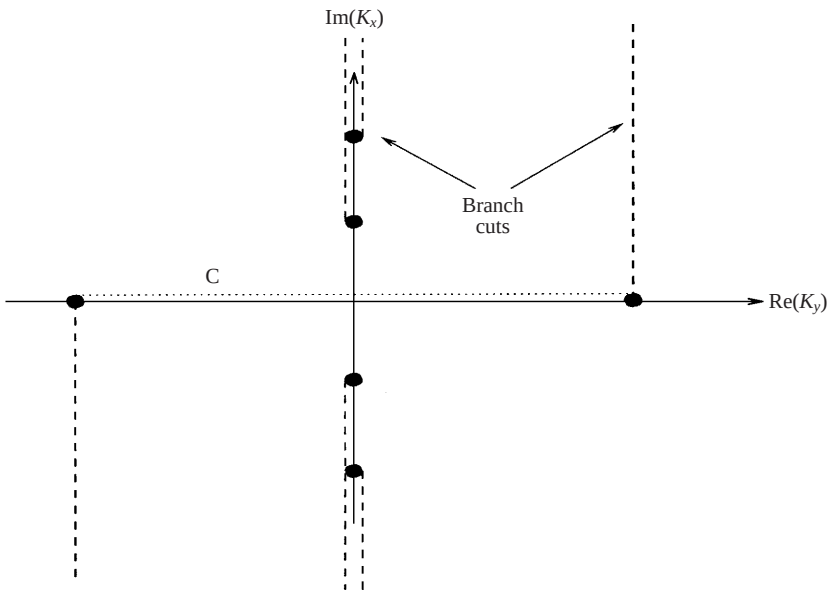

FIGURE 6. Branch cuts in the K_y-plane.

to a convectively growing mode downstream of the point forcing, while closing in the lower half-plane gives two neutral modes upstream. Here we concentrate on the former. It has been previously shown that the K_x mode associated with this growth is given by

$$K_{x_1}^+ = \Omega - \mathrm{i}U^{1/2}(\Omega^2 + K_y^2)^{1/4}(\Omega^2 - (\Omega^2 + K_y^2)^2)^{1/2} + U\frac{\Omega\left(5(\Omega^2 + K_y^2)^2 - \Omega^2\right)}{2(\Omega^2 + K_y^2)^{1/2}} + O(U^{3/2}), \quad (4.25)$$

with $-K_0 < K_y < K_0$. Closing the contour in the upper half-K_x-plane, using the residue theorem (ignoring the branch cut contributions which are small by comparison) and expanding to leading order we have

$$\Psi \sim \frac{\pi}{U^{3/2}} \int_{-K_0}^{K_0} \frac{(\Omega^2 + K_y^2)^{1/4}\, \mathrm{e}^{\mathrm{i}U(K_{x_1}^+ x + K_y y)}}{(\Omega^2 - (\Omega^2 + K_y^2)^2)^{1/2}} \mathrm{d}K_y, \quad (4.26)$$

where $K_{x_1}^+$ is given above. Thus, to determine the large-distance solution we perform a full saddle point analysis in the complex K_y-plane. The analysis is complicated by the presence of six branch cuts defined by the various integrand functions. Indeed, there are branch points at

$$K_y = \pm\mathrm{i}\Omega, \quad K_y = \pm(\Omega - \Omega^2)^{1/2}, \quad K_y = \pm\mathrm{i}(\Omega + \Omega^2)^{1/2}, \quad (4.27)$$

and cuts are taken along the paths shown in figure 6. Note that the second pair of branch points occur at the end points of integration (i.e. $K_y = \pm(\Omega - \Omega^2)^{1/2} = \pm K_0$) and any cuts taken must not interfere with the integration path chosen.

It is now convenient to introduce large-distance scaled x and y variables with

$$x = \frac{X}{U}, \qquad y = \frac{Y}{U^{(1-\alpha)}}, \quad (4.28)$$

with α chosen, for the time being, to lie in the range $1/2 < \alpha < 1$. The integral (4.26) can be recast in the form

$$\Psi \sim \frac{\pi e^{i\Omega X}}{U^{3/2}} \int_{-K_0}^{K_0} g(K_Y) e^{XU^{1/2} f(K_Y,\Omega)} dK_Y, \tag{4.29}$$

with

$$f(K_Y,\Omega) = (\Omega^2 + K_Y^2)^{1/4}(\Omega^2 - (\Omega^2 + K_Y^2)^2)^{1/2} + iU^{\beta} K_Y \frac{Y}{X}, \tag{4.30}$$

$$g(K_Y,\Omega) = \frac{(\Omega^2 + K_Y^2)^{1/4}}{(\Omega^2 - (\Omega^2 + K_Y^2)^2)^{1/2}}, \tag{4.31}$$

and $\beta = \alpha - 1/2$. The choice $1/2 < \alpha < 1$ is significant in determining the leading-order form in the function f above, and the case $0 < \alpha < 1/2$ will be considered later. The integral (4.29) is now in the appropriate form for us to apply a standard saddle-point analysis and so determine the large-distance solution (in the limit $XU^{1/2} \gg 1$).

The saddle points are given by

$$\frac{K_Y}{2}\left(\frac{(\Omega^2 - 5(\Omega^2 + K_Y^2)^2)}{(\Omega^2 + K_Y)^{3/4}(\Omega^2 - (\Omega^2 + K_Y^2)^2)^{1/2}}\right) = -iU^{\beta}\frac{Y}{X} + O(U^{1/2}). \tag{4.32}$$

Thus we have five saddle points, at

$$K_Y = 0, \quad K_Y = \pm\left(\frac{\Omega}{\sqrt{5}} - \Omega^2\right)^{1/2}, \quad \pm i\left(\frac{\Omega}{\sqrt{5}} + \Omega^2\right)^{1/2}, \tag{4.33}$$

and the U^{β} term in (4.32) may be interpreted as the next order correction to these. Obviously the second pair of saddle points can be either imaginary (when $1/\sqrt{5} < \Omega < 1$) or real (when $0 < \Omega < 1/\sqrt{5}$). A thorough analysis of the contour map associated with $f(K_Y,\Omega)$ reveals that the last two saddle points cannot be reached (i.e. it is not possible to deform the contour off the real K_y-axis to pass through them). In fact, to leading order, the last two roots actually lie on the branch cuts, but the correction due to the U^{β} term moves them off. Even so it is still not possible to deform the contour in such a manner as to pass through these saddles and the contribution associated with these points would merely be an end-point contribution. However the other three saddle points can be reached when Ω is within the range $0 < \Omega < 1$, which is associated with the existence of convective instabilities, but it is found necessary to deal with the cases of Ω above and below $1/\sqrt{5}$ separately.

4.4. *The case* $1/\sqrt{5} < \Omega < 1$

To leading order we have one saddle point at the origin and two complex conjugate saddle points, one above and one below the origin. Expanding equation (4.32) to higher order, it is found that the corrected form of the saddle points is now given by

$$\left.\begin{aligned} K_Y &= \frac{2iY\,U^{\beta}\Omega^{1/2}(1-\Omega^2)^{1/2}}{X(5\Omega^2 - 1)} \\ K_Y &= \pm i\left(\Omega^2 - \tfrac{\Omega}{\sqrt{5}}\right)^{1/2} - iU^{\beta}\frac{Y(\Omega/\sqrt{5})^{3/4}}{X(5\Omega^2 - \sqrt{5}\Omega)}. \end{aligned}\right\} \tag{4.34}$$

Examining the contour map associated with these three roots (figure 7) it follows that only the saddle point near to the origin can be reached, and the dominant

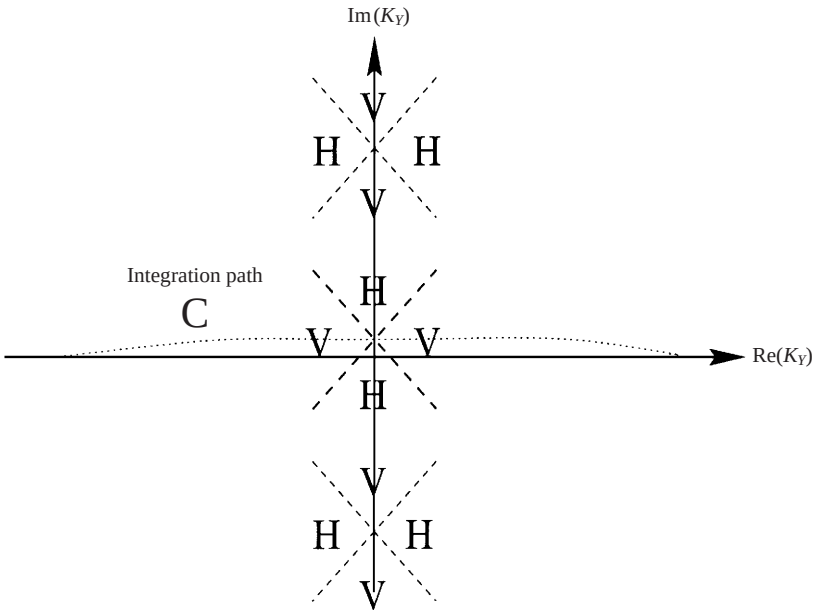

FIGURE 7. Local contour plot for $1/\sqrt{5} < \Omega < 1$. H denotes hill and V valley.

contribution to the integral comes from deforming the contour to pass through this saddle.

At the saddle point, which we denote by s,

$$f(s) \sim \Omega^{3/2}(1-\Omega^2)^{1/2} + \mathrm{i}U^{1/2}\frac{\Omega^2(5\Omega^2-1)}{2} - U^{2\beta}\frac{Y^2\Omega^{1/2}(1-\Omega^2)^{1/2}}{X^2(5\Omega^2-1)}, \tag{4.35}$$

and to leading order

$$\frac{\partial^2 f}{\partial K_Y^2} = \frac{1-5\Omega^2}{2\Omega^{1/2}(1-\Omega^2)^{1/2}} < 0. \tag{4.36}$$

Then by standard saddle-point analysis the dominant flexion contribution is given by

$$\eta(X,Y,T) = \frac{F_0 \exp\left(\mathrm{i}\Omega(X-T) + XU^{1/2}f(s)\right)}{2\sqrt{\pi}U^{3/2}(XU^{1/2})^{1/2}(5\Omega^2-1)^{1/2}\Omega^{1/4}(1-\Omega^2)^{1/4}} \tag{4.37}$$

where $T = U^2 t$ and $f(s)$ is defined above. It is the real part of the function $f(s)$ that controls the growth rate downstream. Indeed it follows that for zero growth rate we must have $\mathrm{Re}(f(s)) = 0$ which, on using formula (4.35), defines a critical angle θ_c,

$$\theta_c = U^{1/2}\Omega^{1/2}(5\Omega^2-1)^{1/2}, \tag{4.38}$$

where $\tan\theta = y/x$. That is, for angles $|\theta| < \theta_c$, we have exponential growth downstream of the driver as usually associated with regions of convective instability. Note that, to perform the analysis for this frequency range it has proven necessary to expand the phase function to second order in U^β. This is a consequence of terms at leading order in U^β cancelling and thus, since $0 < \beta < 1/2$, it also means that we must include the term of order $U^{1/2}$. Next we consider the second frequency region, $0 < \Omega < 1/\sqrt{5}$.

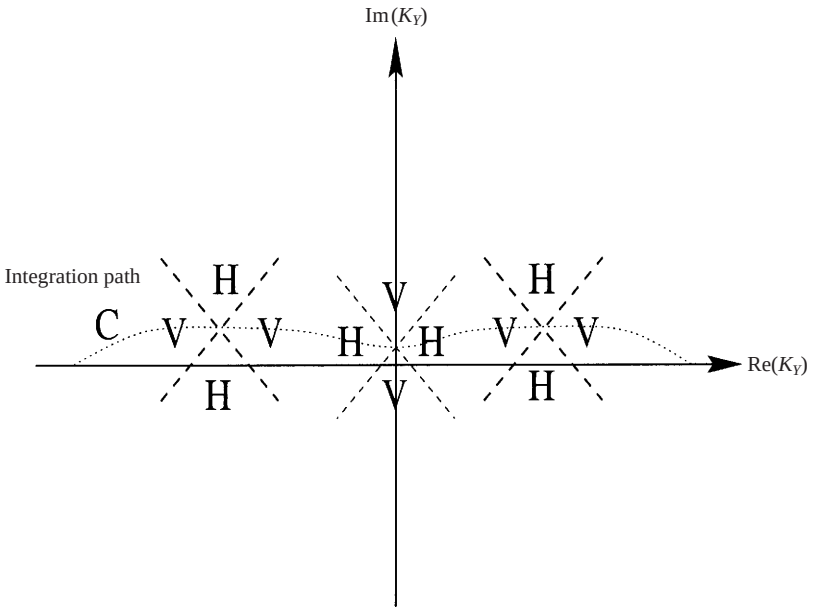

FIGURE 8. Local contour plot for $0 < \Omega < 1/\sqrt{5}$.

4.5. *The case* $0 < \Omega < 1/\sqrt{5}$

To leading order we now have three real saddle points: one at the origin, with one on either side. Expanding equation (4.32) to higher order it is found that the saddle points are now given by

$$\left.\begin{aligned} K_Y &= \frac{2\mathrm{i}Y\,U^{\beta}\Omega^{1/2}(1-\Omega^2)^{1/2}}{X(5\Omega^2-1)}, \\ K_Y &= \pm\left(\frac{\Omega}{\sqrt{5}}-\Omega^2\right)^{1/2} + \mathrm{i}U^{\beta}\frac{Y(\Omega/\sqrt{5})^{3/4}}{X(\sqrt{5}\Omega-5\Omega^2)} \\ &\quad \pm\frac{3U^{2\beta}}{50}\left(\frac{Y}{X}\right)^2\left(\frac{\Omega}{\sqrt{5}}\right)^{6/4}\frac{1}{(\Omega/\sqrt{5}-\Omega^2)^{5/2}}. \end{aligned}\right\} \tag{4.39}$$

Examining the contour map associated with these three roots (figure 8) it follows that the saddle point near to the origin can no longer be reached by traversing from valley to valley. Indeed, it is a complete reversal of the previous situation where now it is the two saddles either side of the origin (s_- and s_+ say) that give a contribution to the integral. Indeed if one were to try and deform the contour in such a manner as to include the saddle at the origin it is unclear which way the integral would have to run – from the lower 'valley' to the upper 'valley', or vice versa – and it could be argued that any attempt would necessarily pass over a local 'hill' region.

It is easily shown that at the origin the function f behaves like

$$f \sim \Omega^{3/2}(1-\Omega^2)^{1/2}, \tag{4.40}$$

and at the saddle points s_- and s_+ one has

$$f \sim 2\left(\frac{\Omega}{\sqrt{5}}\right)^{5/4}. \tag{4.41}$$

The latter function of Ω is larger than the former over $0 < \Omega < 1/\sqrt{5}$, and so the dominant contribution to the integral comes from deforming the contour to pass through the two saddles either side of the origin.

At the saddle points,

$$f_{\pm} \sim 2\left(\frac{\Omega}{\sqrt{5}}\right)^{5/4} \pm \mathrm{i}U^{\beta}\frac{Y}{X}\left(\frac{\Omega}{\sqrt{5}} - \Omega^2\right)^{1/2} - \frac{U^{2\beta}}{10}\left(\frac{Y}{X}\right)^2\left(\frac{\Omega}{\sqrt{5}}\right)^{3/4}\frac{1}{\Omega/\sqrt{5} - \Omega^2}, \quad (4.42)$$

and

$$\frac{\partial^2 f_{\mp}}{\partial K_Y^2} \sim -5(1 - \sqrt{5}\Omega)\left(\frac{\Omega}{\sqrt{5}}\right)^{1/4} < 0, \quad (4.43)$$

where $-$ and $+$ correspond to the saddles s_- and s_+ to the left and right of the origin respectively, as in figure 8. Applying standard saddle-point analysis again, the dominant flexion contribution is now

$$\eta(X, Y, T) = \frac{F_0 \exp\left(\mathrm{i}\Omega(X - T) + XU^{1/2}h(s)\right)}{2\Omega\sqrt{2\pi}U^{3/2}(XU^{1/2})^{1/2}(1 - \sqrt{5}\Omega)^{1/2}} \times \left(\frac{\Omega}{\sqrt{5}}\right)^{1/8}\cos\left(U^{\beta}\frac{Y}{X}\left(\frac{\Omega}{\sqrt{5}} - \Omega^2\right)^{1/2}\right) \quad (4.44)$$

where $T = U^2 t$ and $h(s)$ is defined by

$$h(s) = 2\left(\frac{\Omega}{\sqrt{5}}\right)^{5/4} - \frac{U^{2\beta}}{10}\left(\frac{Y}{X}\right)^2\left(\frac{\Omega}{\sqrt{5}}\right)^{3/4}\frac{1}{\Omega/\sqrt{5} - \Omega^2}. \quad (4.45)$$

Now it is the function $h(s)$ that controls the growth rate downstream, and the critical angle θ_c associated with zero growth rate is now given by

$$\theta_c = 2U^{1/2}(\sqrt{5}\Omega)^{1/4}(\Omega - \sqrt{5}\Omega^2)^{1/2}. \quad (4.46)$$

That is, for angles $|\theta| < \theta_c$, we have exponential growth downstream. Note again that it has been found necessary to expand the saddle-point positions up to order $U^{2\beta}$ allowing for a term in $U^{2\beta}$ to appear in the phase function (with real part $h(s)$). Indeed, as before it is the balance between the leading-order term in Ω and the term of order $U^{2\beta}$, involving X, Y and Ω, that is responsible for defining the critical angle and hence restricting the growth to a wedge-shaped region.

The previous analysis has concentrated strictly on the two cases where $1/\sqrt{5} < \Omega < 1$ and $0 < \Omega < 1/\sqrt{5}$. Both results break down as $\Omega \to 1/\sqrt{5}$. At this value $\partial^2 f/\partial K_Y^2$ vanishes, resulting in a higher-order saddle point, and the previous analysis is insufficient. Geometrically this corresponds to a merging of the three saddle-points at some point near to the origin. Substituting $\Omega = 1/\sqrt{5}$ in equation (4.32) reveals that $K_Y = 0$ now becomes a triple root in the saddle-point equation, to leading order, though the term in U^{β} means that this triple-root position is slightly offset from the origin. In the next section we concentrate on the merging of the three saddle points and demonstrate that equations (4.37) and (4.44) are indeed consistent in an appropriate asymptotic limit.

4.6. *The merging of three saddle points, $\Omega \to 1/\sqrt{5}$*

Near to the critical frequency we write $\Omega = 1/\sqrt{5} + \epsilon\Omega_1$, where $\epsilon \ll 1$. Then an appropriate scaling for K_Y is found to be $K_Y = \epsilon^{1/2}L_Y$. Substituting into the saddle-

point equation (4.32) and expanding to leading order, we find

$$\epsilon^{3/2}L_y(\Omega_1+\sqrt{5}L_Y^2)-\frac{4\mathrm{i}U^\beta}{5}\left(\frac{Y}{X}\right)\left(\frac{1}{5}\right)^{3/4}=0. \tag{4.47}$$

It is the first term that is responsible for the merging of the three roots (as $\Omega_1 \to 0$) and so we choose ϵ such that $\epsilon^{3/2} > U^\beta$. Then we may ignore the term in U^β, which only results in a shift of the merging point away from the origin. To leading order we then have three distinct roots at

$$L_Y = 0 \quad \text{and} \quad L_Y = \pm\left(\frac{-\Omega_1}{\sqrt{5}}\right)^{1/2}. \tag{4.48}$$

Note that for $\Omega_1 > 0$ there are two complex conjugate roots corresponding to the case $1/\sqrt{5} < \Omega < 1$, and for $\Omega_1 < 0$ there are two real roots (either side of the origin), corresponding to the case $0 < \Omega < 1/\sqrt{5}$.

Now we consider the effect of these scalings in the integral (4.29). Writing $N = XU^{1/2}$ we may denote the integral itself (ignoring constant factors) by $I(N)$,

$$I(N)=\int_{-K_0}^{K_0} g(K_Y,\Omega)\mathrm{e}^{Nf(K_Y,\Omega)}\mathrm{d}K_Y, \tag{4.49}$$

where $f(K_Y,\Omega)$ and $g(K_Y,\Omega)$ were previously defined in equation (4.31). Substituting for Ω_1 and L_Y, and expanding in powers of ϵ, it can be shown that

$$\left.\begin{aligned} f(L_Y,\Omega_1) &\sim \frac{2}{5}\left(\frac{1}{5}\right)^{1/4}\left(1+\epsilon\frac{5\sqrt{5}\Omega_1}{4}-\frac{25}{32}\epsilon^2\left(\Omega_1^2+4\sqrt{5}\Omega_1L_Y^2+10L_Y^4\right)\right), \\ g(K_Y,\Omega_1) &\sim \frac{5}{2}\left(\frac{1}{5}\right)^{1/4}, \end{aligned}\right\} \tag{4.50}$$

and thus, for $\epsilon \ll 1$, we have

$$I(N)\sim\frac{5}{2}\left(\frac{1}{4}\right)^{1/4}\epsilon^{1/2}\exp\left(N\frac{2}{5}\left(\frac{1}{5}\right)^{1/4}\right)J(N), \tag{4.51}$$

where

$$J(N)=2\int_0^\infty \exp\left(-aN\left(L_Y^4+\frac{2\Omega_1}{\sqrt{5}}L_Y^2\right)\right)\mathrm{d}L_Y, \tag{4.52}$$

and $a = 25(1/5)^{1/4}\epsilon^2/8$. Writing $L_Y^2 = p$, this may be recast in the form

$$J(N)=\int_0^\infty \frac{\exp\left(-\beta p^2-\gamma p\right)}{p^{1/2}}\mathrm{d}p, \tag{4.53}$$

with

$$\beta = 25(1/5)^{1/4}\epsilon^2N/8 \quad \text{and} \quad \gamma=\frac{2\Omega_1\beta}{\sqrt{5}}. \tag{4.54}$$

From a standard result in Gradshten & Ryzhik (1965, eq. 3.462, p. 337) we have

$$\int_0^\infty x^{v-1}\mathrm{e}^{-\beta x^2-\gamma x}\mathrm{d}x=(2\beta)^{-v/2}\Gamma(v)\mathrm{e}^{\gamma^2/(2\beta)}D_{-v}\left(\frac{\gamma}{\sqrt{2\beta}}\right) \quad \text{for} \quad \mathrm{Re}(v,\beta)>0. \tag{4.55}$$

Here Γ is the usual Gamma function and D_{-v} is a parabolic cylinder function (defined

in Gradshten & Ryzhik, § 9.24). Thus setting $v = 1/2$ yields $J(N)$ in the form

$$J(N) = \left(\frac{1}{2\beta}\right)^{1/4} \sqrt{\pi} \exp\left(\frac{\Omega_1^2\beta}{10}\right) D_{-1/2}\left(\frac{2\Omega_1\beta^{1/2}}{\sqrt{10}}\right), \tag{4.56}$$

and combining this with (4.51),

$$I(N) \sim \frac{5\sqrt{\pi}}{2}\left(\frac{1}{8\beta}\right)^{1/4} \epsilon^{1/2} \exp\left(N\frac{2}{5}\left(\frac{1}{5}\right)^{1/4} + \frac{\Omega_1^2\beta}{10}\right) D_{-1/2}\left(\frac{2\Omega_1\beta^{1/2}}{\sqrt{10}}\right), \tag{4.57}$$

with

$$\eta(X, Y, T) = \frac{F_0 e^{i\Omega(X-T)}}{4\pi U^{3/2}} I(N). \tag{4.58}$$

Since the parabolic cylinder function $D_{-1/2}$ is regular at the origin, it follows immediately that the integral $I(N)$ (and thus the flexion η) is regular as $\Omega_1 \to 0$ (corresponding to $\Omega \to 1/\sqrt{5}$). Indeed the singularities that arose within the solutions, for $\Omega < 1/\sqrt{5}$ and $\Omega > 1/\sqrt{5}$, as $\Omega \to \mp 1/\sqrt{5}$ respectively, were a consequence of the merging of the three saddle points. It is, however, possible to recover the singular behaviour of both solutions when limits are taken in an appropriate fashion.

If we take the limit $\Omega_1 \to \infty$ and then let $\Omega_1 \to 0$ we should recover the singular behaviour associated with (4.37) as $\Omega \to 1/\sqrt{5}$. Similarly if we take the limit $\Omega_1 \to -\infty$ and then let $\Omega_1 \to 0$ we should recover the singular behaviour associated with (4.44) as $\Omega \to 1/\sqrt{5}$. That is, by looking at the large-frequency solutions ($\Omega_1 \to \pm\infty$) we obtain the appropriate asymptotic form of solution. Then letting $\Omega_1 \to 0\pm$, we obtain the correct singular form of solution near the critical frequency.

Before we take the limits $\Omega_1 \to \pm\infty$ we need the preliminary result from Gradshten & Ryzhik (eq. 9.246, p. 1065) that

$$\left.\begin{aligned} D_{-1/2}(z) &\sim e^{-z^2/4} z^{-1/2} \quad \text{as} \quad z \to \infty, \ \arg(z) < 3\pi/4, \\ D_{-1/2}(z) &\sim \frac{i\sqrt{2\pi}}{\Gamma(1/2)} e^{z^2/4} z^{-1/2} \quad \text{as} \quad z \to -\infty, \ \pi/4 < \arg(z) < 5\pi/4. \end{aligned}\right\} \tag{4.59}$$

Taking the asymptotic form for $D_{-1/2}$ as $\Omega_1 \to \infty$, applying it in (4.57), and then letting $\Omega_1 \to 0$, it is found that

$$I(N) \sim \frac{5^{1/8}\sqrt{\pi}\exp\left(2N(1/\sqrt{5})^{1/2}/5\right)}{\epsilon^{1/2} N^{1/2} \Omega_1^{1/2}}. \tag{4.60}$$

It is easily shown that the singularity which arises from (4.37) is precisely that in (4.60).

Taking the asymptotic form for $D_{-1/2}$ as $\Omega_1 \to -\infty$, applying it in (4.57), and then letting $\Omega_1 \to 0$, it is found that

$$I(N) \sim \frac{5^{1/8}\sqrt{\pi}\exp\left(2N(1/\sqrt{5})^{1/2}/5\right)}{\epsilon^{1/2} N^{1/2} (-\Omega_1)^{1/2}} \sqrt{2}. \tag{4.61}$$

Again, the singularity from (4.44) is precisely (4.61). Note that the asymptotic forms for the solutions as given by (4.60) and (4.61) differ by a factor of $\sqrt{2}$. This is a result of the difference in behaviour of the parabolic cylinder function $D_{-1/2}(z)$ in the limits $z \to \pm\infty$. It is therefore especially comforting that both sets of results actually agree

in the correct limit with the forms of solution derived within equations (4.37) and (4.44) for the large-distance flexion response.

4.7. *Outside the wedge region* ($0 < \alpha < 1/2$)

The choice $\alpha < 1/2$ means that the original spatial variables (x, y) are related to their large-distance scaled counterparts (X, Y) by

$$\tan\theta = \frac{y}{x} = \frac{Y}{X}U^{\alpha}, \tag{4.62}$$

where, for X and $Y = O(1)$, the angle θ now lies outside the critical angles θ_{c_i} which allow convective growth. That is, the choice $\alpha < 1/2$ corresponds to the solution outside the wedge region derived in the previous sections. With this choice of α the integral (4.29) can be written in the form

$$\Psi \sim \frac{\pi e^{i\Omega X}}{U^{3/2}} \int_{-K_0}^{K_0} g(K_Y) e^{XU^{\alpha}F(K_Y,\Omega)} dK_Y, \tag{4.63}$$

with

$$\left.\begin{aligned} F(K_Y,\Omega) &= iK_Y\tfrac{Y}{X} + U^{\gamma}(\Omega^2 + K_Y^2)^{1/4}(\Omega^2 - (\Omega^2 + K_Y^2)^2)^{1/2}, \\ g(K_Y,\Omega) &= \frac{(\Omega^2 + K_Y^2)^{1/4}}{(\Omega^2 - (\Omega^2 + K_Y^2)^2)^{1/2}}, \end{aligned}\right\} \tag{4.64}$$

and $\gamma = 1/2 - \alpha$. Now it is the term in Y/X which dominates the phase function $F(K_Y, \Omega)$ for this choice of α. The saddle points are now given by

$$\frac{Y}{X}\left(\Omega^2 + K_Y^2\right)^{3/4}\left(\Omega^2 - (\Omega^2 + K_Y^2)^2\right)^{1/2} = U^{\gamma} i\frac{K_Y}{2}\left(\Omega^2 - 5(\Omega^2 + K_Y^2)^2\right), \tag{4.65}$$

and, to leading order are now coincident with the branch points, at

$$K_Y = \pm i\Omega, \quad K_Y = \pm(\Omega - \Omega^2)^{1/2}, \quad \pm i(\Omega + \Omega^2)^{1/2}, \tag{4.66}$$

with the term in U^{γ} providing a small correction away from the associated branch points. However, a careful examination of the contour map of $F(K_Y, \Omega)$ (figure 9) reveals that it is no longer possible to deform the integration path, so as to pass through any of these saddle points. That is, the leading-order contribution to the integral now comes from the end points ($K_Y = \pm K_0$) of the integration range.

Again we denote the integral for the large-distance solution by

$$I(M) = \int_{K_0}^{K_0} g(K_Y, \Omega) e^{MF(K_Y,\Omega)} dK_Y, \tag{4.67}$$

where $M = XU^{\alpha} \gg 1$ now. The dominant contribution to the integral comes from the end points,

$$I(M) \sim \frac{1}{2K_0^{1/2}\Omega^{1/4}}\left(J_1(M) + J_2(M)\right), \tag{4.68}$$

where

$$J_1(M) = \int_0^{K_0} \frac{\exp\left(iMK_Y(Y/X)\right)}{(K_0 - K_Y)^{1/2}} dK_Y, \quad J_2(M) = \int_0^{K_0} \frac{\exp\left(-iMK_Y(Y/X)\right)}{(K_0 - K_Y)^{1/2}} dK_Y. \tag{4.69}$$

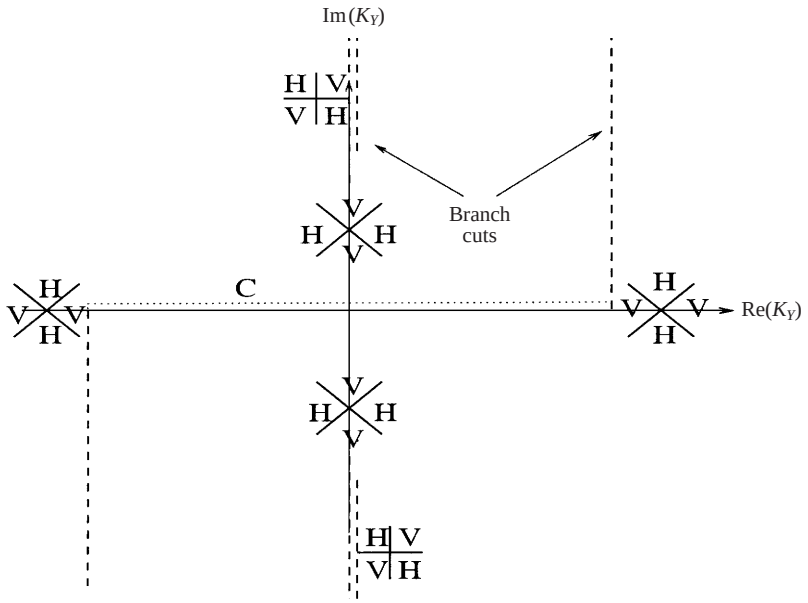

FIGURE 9. Contour plot of $F(K_Y, \Omega)$ when $\alpha < 1/2$.

Both of these integrals may be evaluated exactly, and

$$I(M) \sim \frac{\sqrt{\pi}}{2K_0^{1/2}\Omega^{1/4}} \left(\frac{\exp\left(\mathrm{i}(M(Y/X)K_0 - \pi/4)\right)}{(MY/X)^{1/2}} + \frac{\exp\left(-\mathrm{i}(M(Y/X)K_0 - \pi/4)\right)}{(MY/X)^{1/2}} \right). \tag{4.70}$$

Combining this with (4.63) it follows that the large-distance flexion response outside the wedge region is given by

$$\eta(X, Y, T) = \frac{F_0 \exp\left(\mathrm{i}\Omega(X - T)\right) \cos\left(U^{\alpha} Y K_0 - \pi/4\right)}{U^{3/2} 4\sqrt{\pi} (Y U^{\alpha})^{1/2} (\Omega - \Omega^2)^{1/4} \Omega^{1/4}}. \tag{4.71}$$

Thus, outside the wedge region the large-distance solution takes the form of a modulated neutral mode. Comparing this with the results for the convectively unstable modes, (4.37) and (4.44), the solution now decays like $1/(Y U^{\alpha})^{1/2}$ as opposed to $1/(X U^{1/2})^{1/2}$ for the unstable modes.

4.8. *Neutral mode behaviour upstream of the driver*

All of the previous behaviour is found downstream of the driver and will dominate any large time/distance solution. Upstream of the driver there are only two neutral modes (at worst), one with $\mathrm{Re}(k_x) > 0$ and one with $\mathrm{Re}(k_x) < 0$. In fact closing the contour c of the integral (4.24) in the lower half-plane it can be shown that the resulting neutral modes combine to form

$$\eta(X_1, Y_1, T) = \frac{2F_0}{3\pi U (Y_1 U^{1/3})} \exp\left(-\mathrm{i}\Omega \left(T + \frac{2X_1 U^{1/3}}{3} \right) \right) \sin\left(U^{1/3} Y_1 K_0\right) \times \sin\left(X_1 + 5(|X_1| U^{1/3}) U^{1/3} K_0^2/6\right), \tag{4.72}$$

where $(x, y) = U^{-2/3}(X_1, Y_1)$ now, with $U^{1/3}|X_1|$, $U^{1/3} Y_1 \gg 1$, and $Y_1/X_1 = O(1)$. It transpires that the case $Y_1/X_1 \sim O(U^{1/3})$ requires separate consideration. Thus

writing $Y_1 = U^{1/3}Y_2$ we find the large-distance flexion response then given by

$$\eta(X_1, Y_2, T) = \frac{-\mathrm{i}F_0}{3\pi U}\sqrt{\frac{6\pi}{5}}\frac{\exp\left(-\mathrm{i}\Omega\left(T + \frac{2}{3}X_1U^{1/3}\right)\right)}{(|X_1|U^{2/3})^{1/2}} \times \sin\left(X_1 - \frac{3}{10}U^{2/3}|X_1|\frac{Y_2^2}{X_1^2} + \frac{\pi}{4}\right), \quad (4.73)$$

with $U^{2/3}|X_1| \gg 1$. The reason for the two different types of behaviour is the presence of a stationary point of the integral at $K_Y = \pm\frac{3}{5}Y/(XU^{1/3})$ (where $k_y = UK_Y$ as usual). When this lies within the integration range of K_Y (i.e. $|K_Y| < K_0$) the latter result is obtained. Otherwise the former result is the correct one. Physically the appearance of two different types of behaviour gives rise to another critical angle, θ_{c2}, say, defined by

$$\theta_{c2} \sim \frac{y}{|x|} = \frac{5U^{1/3}}{3}\left(\Omega - \Omega^2\right)^{1/2}, \quad (4.74)$$

which is now found upstream of the driver. For values of $\theta > \theta_{c2}$ we have a neutral mode of the form (4.72), with spatial decay like $1/X_1$, and for values of $\theta < \theta_{c2}$ we have (4.73), with spatial decay $1/X_1^{1/2}$ (so that there is again a thin wedge region with a different decay rate).

The two equations (4.72) and (4.73) were derived from (4.24) by closing the contour c in the lower half-k_x-plane and using the neutral mode forms in (4.22), which are valid for $k_y \sim O(U)$. However the integral (4.24) has a restricted integration range given by $|k_y| < UK_0$, within which there exists convective growth downstream. Upstream of the driver there is no reason to truncate the integral in this manner. Indeed there may be (and are) other neutral modes outside the region $(-UK_0, UK_0)$ which must also be accounted for. A careful analysis reveals that for $UK_0 < k_y < U^{2/3}K_1$ there are two neutral modes upstream, and for $U^{2/3}K_1 < k_y < U^{2/3}K_2$ there is one neutral mode (and one exponentially decaying mode), where K_1 and K_2 are given by

$$\left.\begin{aligned} K_1 &= \left(\frac{2}{3}\right)^{1/3}\left(\frac{3}{5}\right)^{5/6} - U^{1/3}\left(\frac{2}{3}\right)^{1/2}\Omega - U^{2/3}\frac{5\Omega^2}{12}\left(\frac{3}{2}\right)^{1/3}\left(\frac{5}{3}\right)^{5/6}, \\ K_2 &= \left(\frac{2}{3}\right)^{1/3}\left(\frac{3}{5}\right)^{5/6} + U^{1/3}\left(\frac{2}{3}\right)^{1/2}\Omega - U^{2/3}\frac{5\Omega^2}{12}\left(\frac{3}{2}\right)^{1/3}\left(\frac{5}{3}\right)^{5/6}. \end{aligned}\right\} \quad (4.75)$$

Unfortunately for both these regions it is no longer possible to obtain the k_x-modes as explicit functions of k_y, the resulting dispersion relation being now of the form

$$K^5 - K_X^2 = -2U^{1/3}\Omega K_x + U^{2/3}\Omega^2 + U^{4/3}\Omega^2 K \quad (4.76)$$

where now $(k_x, k_y, k) = U^{2/3}(K_X, K_Y, K)$. Thus, it is impossible to find an asymptotic form of solution as before, and the solution now requires a numerical approach instead. The current paper has concentrated on the asymptotic form of the convectively unstable (and most dominant) mode and as such we simply note that the form given earlier in this section for the upstream neutral modes is not the complete solution, and must be complemented by the numerically calculated modes as well.

5. Conclusion

The paper considers the three-dimensional problem of a fluid-loaded elastic plate with a uniform mean flow which is subject to a localized point forcing. The approach

adopted is similar to that taken by Crighton & Oswell (1991), who examined the two-dimensional problem of a line-forced elastic plate, and Peake (1997), who included transverse curvature effects; and results are compared accordingly. In particular, the usual one-dimensional Briggs–Bers method for determining the large-time solution is modified to deal with the two-dimensional causal structural response problem that now arises.

The first part of the paper concentrates on the existence of absolute instability and a systematic method for determining the threshold is derived. It was demonstrated by Crighton & Oswell that absolute instability occurs for the one-dimensional structural problem when three modes coalesce. Mathematically this corresponds to an inflection point of the dispersion function and the natural extension of this for the two-dimensional structural problem involves the vanishing of the discriminant (i.e. limiting case of the existence of a saddle point). It is demonstrated analytically (using the discriminant) and via a numerical argument that the flow becomes absolutely unstable for normalized flow speeds $U > U_c$, where $U_c \approx 0.074$ is the same value identified by Crighton & Oswell for the line-driven problem. It is shown that this critical velocity occurs when the transverse Fourier wavenumber k_y vanishes and that for larger values of k_y the absolute instability threshold is larger than U_c. Indeed, for small values of k_y, one can derive an expansion for the associated critical velocity U_y (formula (3.15)) with $U_y > U_c$ when $k_y \neq 0$.

The second part of the paper concentrates on the case $U < U_c$ and is concerned with the existence of convectively stable and unstable flow. It is demonstrated that convective instability only exists for small values of k_y ($O(U)$) and asymptotic forms for the turning points and branch points of the dispersion function are derived, with k_y considered as given and small. In the limit as $k_y \to 0$ the results of Crighton & Oswell (1991) are recovered. For small values of $k_y < U/2$ there exists an extra 'hoop' region of stability which was not present in the Crighton & Oswell model, but did arise in Peake's (1997) problem, when transverse curvature effects were included.

The region lying between the main stability branch and the stability hoop is identified as a region of convective instability, and convective instability thresholds are found in the form $\omega(k_y, U)$ (equations (4.20) and (4.21)), with $k_y < U/2$, and in the form $k_y(\omega, U)$ (equation (4.23)), with $0 < \omega < U^2$, both of which agree with the results of Crighton & Oswell as $k_y \to 0$. Using the small U and k_y approximations within the convective region, it is possible to obtain asymptotic forms for the various modes in the form $k_x(k_y, \omega, U)$. Applying the Briggs–Bers type of analysis we find a convectively growing mode and an evanescent mode located downstream of the driver and two neutral modes upstream of the driver.

The large-distance flexion response downstream of the driver is derived within the convectively unstable region using a saddle-point analysis, and it is found that convective growth only occurs within a wedge-shaped region of angle $O(U^{1/2})$. It transpires that the flexion response takes two possible forms, depending on whether $\omega < U^2/\sqrt{5}$ or $\omega > U^2/\sqrt{5}$, and two forms for the wedge boundary are derived accordingly. A closer inspection reveals that as $\omega \to U^2/\sqrt{5}$ there is actually a merging of three saddle points, resulting in a caustic type of behaviour. Performing a careful analysis near to this merging point, the flexion response is derived in terms of parabolic cylinder functions and it is demonstrated how the asymptotic forms (4.37) and (4.44) may be recovered when an appropriate limit is taken. Finally, the solution outside the wedge region is derived and takes the form of a modulated neutral mode.

For completeness we also derive the upstream neutral modes resulting from the convective truncation of the flexion integral. Again there are two different decay rates

found, depending on whether one is inside or outside a wedge region of $O(U^{1/3})$. However there are other neutral modes upstream of the driver which should also be included but lie outside the convective region. Such modes are impossible to obtain asymptotically and we simply note that the upstream asymptotic form derived here may not account for all of the large-distance solution.

REFERENCES

Abrahams, I. D. & Wickham, G. R. 1994 On the stability of a forced elastic surface under a uniformly moving fluid. Paper at EUROMECH 316.

Bers, A. 1983 Space-time evolution of plasma instabilities – absolute and convective. In *Handbook of Plasma Physics* (ed. M. N. Rosenbluth, R. Z. Sagdeev), vol. 1, pp. 451–517. North-Holland.

Brazier-Smith, P.R. & Scott, J. F. 1984 Stability of fluid flow in the presence of a compliant surface. *Wave Motion* **6**, 547–560.

Briggs, R. J. 1964 *Electron-stream Interaction with Plasmas*. Monograph No. 29. MIT Press.

Benjamin, T. B. 1960 Effects of a flexible boundary on hydrodynamic stability. *J. Fluid Mech.* **9**, 513–532.

Benjamin, T. B. 1963 The threefold classification of unstable disturbances in flexible surfaces bounding inviscid flows. *J. Fluid Mech.* **16**, 436–450.

Cairns, A. D. 1979 The role of negative energy waves in some instabilities of parallel flows. *J. Fluid Mech.* **92**, 1–14.

Crighton, D. G. & Oswell, J. E. 1991 Fluid loading with mean flow. I. Response of an elastic plate to localised excitation. *Phil. Trans. R. Soc. Lond.* **335**, 557–592.

Gradshten, I. S. & Ryzhik, I. M. 1965 *Table of Integrals Series and Products*. Academic.

Landahl, M. T. 1962 On the stability of a laminar incompressible boundary layer over a flexible surface. *J. Fluid Mech.* **13**, 609–632.

Lucey, A. D. & Carpenter, P. W. 1992 A numerical simulation of the interaction of a compliant wall and inviscid flow. *J. Fluid Mech.* **234**, 121–146.

Peake, N. 1997 On the behaviour of a fluid-loaded cylindrical shell with mean flow. *J. Fluid Mech.* **338**, 387–410.